Hindawi Publishing Corporation
Journal of Catalysts
Volume 2013, Article ID 178512, 9 pages
http://dx.doi.org/10.1155/2013/178512

Research Article

Tuning the Photocatalytic Activity and Optical Properties of Mesoporous TiO_2 Spheres by a Carbon Scaffold

Leticia F. Velasco,[1,2] Marta Haro,[1] Julien Parmentier,[2] Roger Gadiou,[2] Cathie Vix-Guterl,[2] and Conchi O. Ania[1]

[1] *Instituto Nacional del Carbón (INCAR), Consejo Superior de Investigaciones Científicas (CSIC), C/ Francisco Pintado Fe 26, 33011 Oviedo, Asturias, Spain*
[2] *Institut de Science des Matériaux de Mulhouse (IS2M), LRC CNRS 7228 UHA, 68057 Mulhouse, France*

Correspondence should be addressed to Leticia F. Velasco; leticia@incar.csic.es

Received 9 August 2012; Accepted 23 October 2012

Academic Editor: Hicham Idriss

The photoelectrochemical response and catalytic efficiency towards phenol photooxidation of mesoporous titania particles with spherical morphology have been explored. The catalysts were synthesized in two different arrangements using carbon spheres in a dual role as support and morphology director: hollow spherical titania particles and dense structures where the titania shell is surrounding a carbon core. Although the synthesized titania hollow spheres exhibited a similar photoelectrochemical behavior and optical properties than commercial P25, they showed a better photocatalytic response towards phenol photo-oxidation in terms of pollutant mineralization. This behavior cannot be explained in terms of the crystallinity (found to be higher for P25) and has been attributed to both confinement effects in the mesoporosity of these catalysts as well as to the spherical morphology of titania particles. The spherical arrangement of the titania surface would favor the fast motion of the charge carriers and minimize recombination processes. On the other hand, no clear contribution of the carbon phase to the enhanced photocatalytic response, since quite similar performance is observed for the hollow spheres and the core/shell composite. However, separation and filtration of the catalysts become easier for the carbon/titania composite, thereby improving the so-called practical efficiency.

1. Introduction

Triggered by the rising interest in the development of advanced oxidation processes (AOP) for wastewater remediation, heterogeneous photocatalysis has received much attention in the last years [1, 2]. Particularly, extensive research is being carried out on the development of novel synthetic routes to improve the photocatalytic activity of conventional semiconductors—mostly TiO_2 and ZnO—and ideally achieving the complete degradation (mineralization) of recalcitrant pollutants both in liquid and gas phase. The low efficiency of AOP based on heterogeneous photocatalysis is mainly due to high surface recombination rates of the charge carriers, low efficiency under visible light, separation (filtration), and recovery and reutilization of the fine photocatalyst powders [3, 4]. To overcome all these issues, different approaches are being considered such as doping with transition metal and nonmetal ions, surface sensitization of dyes, design of nanostructured photocatalysts with controlled morphology, or immobilization on appropriate substrates [2, 5–8].

In this regard, the enhanced photocatalytic performance of carbon/semiconductor composites has been reported over a variety of carbon sources, forms, and morphologies (powders, fibers, foams, and cloths), using different synthetic routes for the catalyst preparation (mechanical mixture, coating by liquid impregnation, hydrothermal process, chemical vapor deposition, etc.) [9–11]. The potential role of carbon materials in the enhanced photocatalytic response of the carbon/semiconductor composites has not yet been fully understood but is generally attributed to either single or collective factors traditionally associated to visible light absorption of the composites, synergy effects due to textural features (i.e., surface area), strong interfacial electronic

effects, and more recently the self-photochemical activity of certain carbon materials under UV light [2, 9–13].

On the other hand, the structural properties of the semiconductor also control its photocatalytic activity (i.e., due to crystal defects and recombination lifetime), and the development of synthetic routes with potential control over the semiconductor characteristics (i.e., topology, morphology, particle size, and crystallinity) has long attracted much attention [2, 14, 15].

Bearing all this in mind, the combination of a carbon matrix and TiO_2 with tailored architectures opens up the possibility to obtain catalysts with enhanced photoactivity. The aim of this study was to explore the photocatalytic activity of a series of catalysts prepared with different morphology and composition. For this purpose, carbon/titania composites were prepared using colloidal carbon spheres obtained by hydrothermal carbonization of polysaccharides. The dual role of the carbon spheres as support and scaffold (morphology director) enabled to obtain hybrid carbon/titania catalysts in a core-shell structure, as well as titania hollow spheres.

Although the synthesis of such materials has already been described in the literature [15, 16], their catalytic and photoelectrochemical behavior has been scarcely investigated. Most studies report the details on the synthesis, whereas few works on the photooxidation ability of such materials deal with nonrecalcitrant compounds (i.e., dyes) [17–20]. Herein, we have explored the photocatalytic activity of these core/shell and hollow sphere structures towards the photooxidation of a recalcitrant aromatic compound (i.e., phenol), aiming at throwing some light on the role of titania morphology and porosity of the photooxidation yield from a mechanistic point of view.

2. Experimental

2.1. Materials Synthesis. In a typical synthesis of the carbon spheres used as support, about 250 mL of 0.5 M glucose solution were placed in a 400 mL Teflon-lined autoclave, and maintained at 180°C for 10 hours to allow hydrothermal carbonization of the polysaccharide. The brownish solid obtained was isolated from the solution by centrifugation, washed several times with water and ethanol and dried at 60°C. This material was labeled as CS. The titania coating film was incorporated by dispersing 0.4 g of the carbon support in 200 mL of an ethanol/acetonitrile (3 : 1) solution and adding 2 mL of titanium (IV) isopropoxide. After 2 h stirring, the solvents were removed by centrifugation. Finally, C/TiO_2 core-shell spheres were redispersed in 64 mL of distilled water and 1.2 mL of NH_3 (aq) were added to the solution before carrying out hydrothermal treatment in an autoclave at 180°C for 12 h [16]. After washing and drying, the resulting carbon/titania composite was labeled as CSTi. Additionally, CSTi composite was calcined at 550°C for 2 hours to remove the carbon matrix and allow the development of photoactive crystalline phase of titania (anatase). Calcined samples were labeled as HSTi. For comparison reasons, the commercially available TiO_2 (P25 from Degussa, Evonik, Germany) was employed as a reference photocatalyst.

2.2. Physicochemical, Textural, and Structural Characterization. Textural characterization was carried out by measuring the N_2 adsorption isotherms at −196°C in an automatic apparatus (Micrometrics ASAP 2010). Before the experiments, the samples were outgassed under primary vacuum at 120°C overnight. The isotherms were used to calculate specific surface area S_{BET}, total pore volume V_T, and pore volumes using the NLDFT method. The morphology of the samples was characterized by transmission electron microscopy (TEM) on a Philips CM200 at 200 kV. The point of zero charge (pH_{PZC}) was determined by the mass titration method as indicated elsewhere [21] (using a pHmeter Basic 20+, Crison, Spain). X-ray diffraction (XRD) patterns were recorded on a Bruker instrument (D8 Advance) operating at 40 kV and 40 mA and using CuKα (λ = 0.15406 nm) radiation. UV-Vis diffuse reflectance (DRUV) spectra were recorded on a Shimadzu spectrometer (UV-2501) equipped with an integrating sphere and using $BaSO_4$ as a blank reference.

2.3. Photocatalytic and Photoelectrochemical Performance. Phenol photodegradation experiments under UV irradiation were followed by means of kinetics studies from batch experiments at room temperature. Briefly, about 0.5 g L^{-1} of catalyst was placed in a photoreactor of 400 mL capacity, containing an aqueous solution of phenol of initial concentration 100 mg L^{-1} (solution pH ca. 6 units). For comparison purposes, the mass of the composite was adjusted to provide the same fraction of titanium oxide used in the three catalysts. The UV irradiation source was provided by a high pressure mercury lamp (125 W, Helios Italquartz), vertically suspended in a cylindrical, double-walled quartz jacket cooled by flowing water, immersed in the solution. The water cell was used to control the temperature during the experiments, preventing any overheating of the suspension due to the irradiation. The suspensions were stirred (500 rpm) during the UV irradiation and small aliquots of the solution (~1 mL) were taken out at regular time intervals; phenol and its degradation intermediates were analyzed by reverse-phase HPLC (Spherisorb C18, 125 mm × 4 mm), using a methanol-water mixture (5 : 95) as mobile phase, and a photodiode array detector. The samples were previously filtered using regenerated cellulose filter having mean pore size of 0.45 μm. Total Organic Carbon (TOC) of the solution was also measured in a TOC-V analyzer (Shimadzu).

The photolysis (noncatalyzed degradation reaction) of phenol was performed through the irradiation of an aqueous solution of phenol in the absence of catalyst. Dark adsorption (in the absence of UV irradiation) was also carried out under the same experimental conditions than UV irradiation, in order to evaluate the contribution of adsorption. All the experiments were done in triplicate and demonstrated to be reproducible; reported data represent the average values.

The photoelectrochemical behavior of the catalysts was investigated in a standard three electrodes system, using saturated calomel (SCE) and platinum wire as reference and counter electrodes, respectively. The working electrode consisted of a thin film of the catalyst deposited on indium tin oxide (ITO) conductive glass slides by spin coating, dried at 100°C overnight and subsequently annealed in a

Table 1: Main physicochemical characteristics of the synthesized photocatalysts obtained from gas adsorption data and elemental analysis.

	CS	CSTi	HSTi	P25
S_{BET} $\left[m^2\,g^{-1}\right]$	10	80	74	57
V_{Total} $\left[cm^3\,g^{-1}\right]^a$	0.02	0.19	0.21	0.14
$V_{Micropores}$ $\left[cm^3\,g^{-1}\right]^b$	0.004	0.002	0.005	0.006
$V_{Mesopores}$ $\left[cm^3\,g^{-1}\right]^b$	0.01	0.09	0.16	0.08
C [wt.%]	70.4	35.9	—	—
H [wt.%]	4.6	2.3	—	—
O [wt.%]	24.8	23.9	—	—

[a]Evaluated at p/p_0 0.99.
[b]Evaluated from NLDFT method.

muffle furnace at 450°C for 30 min in air. The prepared electrodes were immersed in a solution containing 0.1 M Na_2SO_4 (pH 2) as inert electrolyte, placed in front of the UV lamp and allowed to equilibrate for ca. 1 hour. The photoelectrochemical response of the thin film electrodes upon on and off illumination was recorded on an electrochemical workstation applying a linear voltage sweep between −600 and +600 mV versus SCE at a scan rate of 20 mV/s. The transient photocurrent response of the electrodes at a fixed bias potential was also recorded for several times to evaluate the electron transfer mechanism and reproducibility of the prepared electrodes.

3. Results and Discussion

3.1. Characterization of the Catalysts. A detailed characterization of the physicochemical features of the synthesized catalysts was carried out, and it is presented in Table 1 and Figure 1. The prepared carbon spheres (sample CS) display a low surface area (S_{BET} = 10 m^2/g) and acidic (hydrophilic) character (point of zero charge about 3.8 pH units). Perfect spherical morphology with uniform particle size of the carbon spheres was confirmed by TEM (Figure 2); these parameters are in good agreement with previous studies in the literature describing the hydrothermal carbonization of polysaccharides at varied conditions [15, 22].

On the other hand, CSTi showed a type IV nitrogen adsorption isotherm, characteristic of mesoporous materials, with a capillary condensation step starting at relative pressures above 0.7. The hysteresis loop displayed a curvature (inflection point) at relative pressures above 0.9, which suggests the presence of a bimodal mesopore size distribution. This was further confirmed by NLDFT method applied to the gas adsorption data, with an average pore size distribution centered at ca. 3 and 10 nm.

A similar shape was obtained after the calcination step carried out to burn out the carbon matrix (sample HSTi), indicating that the titania hollow spheres still keep the mesoporous structure of pristine CSTi sample. This confirmed that the mesoporosity is mainly associated to the titania layer, and that the texture of the titania layer which was not significantly altered during the removal of the carbon

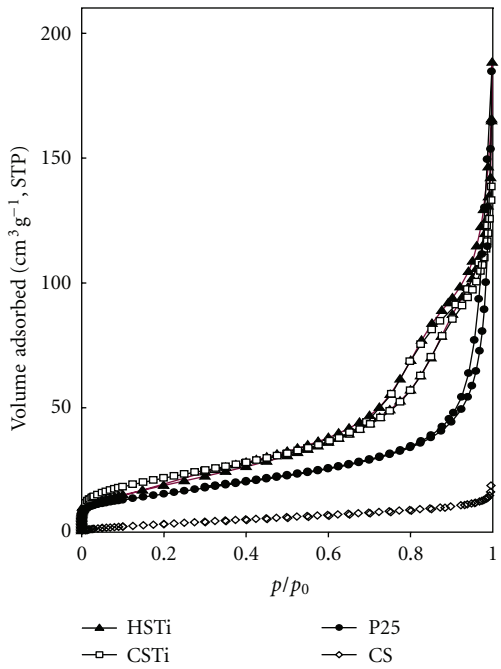

Figure 1: N_2 adsorption isotherms at −196°C of the synthesized photocatalysts.

spheres. This seems reasonable as the void space inside the hollow spheres (Figure 2(d)) is too large to be measured by N_2 adsorption at −196°C. Comparatively, commercial titania powders display a nonporous character, as evidenced by the type II nitrogen adsorption isotherm (Figure 1).

According to literature [23], carbon materials obtained by hydrothermal carbonization of saccharides are characterized by two distinct chemical regions in a core-shell configuration. The hydrophobic core is mainly constituted of cross-linked furanic and ether/keto-aliphatic chains, whereas the hydrophilic shell contains a high density of oxygen surface groups of acidic nature (i.e., hydroxyl, carbonyl, or carboxylic). The infrared spectra (not shown) and elemental analysis (Table 1) of herein synthesized carbon spheres confirmed the abundance of oxygen-containing surface functionalities. Such unusual chemical composition is of paramount importance to control the grafting of the titania precursor to the carbon surface during the synthesis of the carbon/titania composite.

Indeed, TEM images (Figure 2(b)) showed that sample CSTi displays a spherical morphology, which indicates the grafting of titanium oxide in the O-moieties of the carbon spheres during the sol-gel process, with no appreciable modification of size of the carbon spheres (see circles depicted in Figures 2(a) and 2(b)). Thus, CSTi has a core/shell structure where the shell is constituted by a homogenous titania thin layer surrounding the carbon core. The carbon : titania ratio in the resulting composite was 48 : 52 wt.%, as measured by calcination of the sample. Moreover, the removal of the carbon scaffold by calcination at moderate temperature rendered titania particles in a hollow sphere configuration

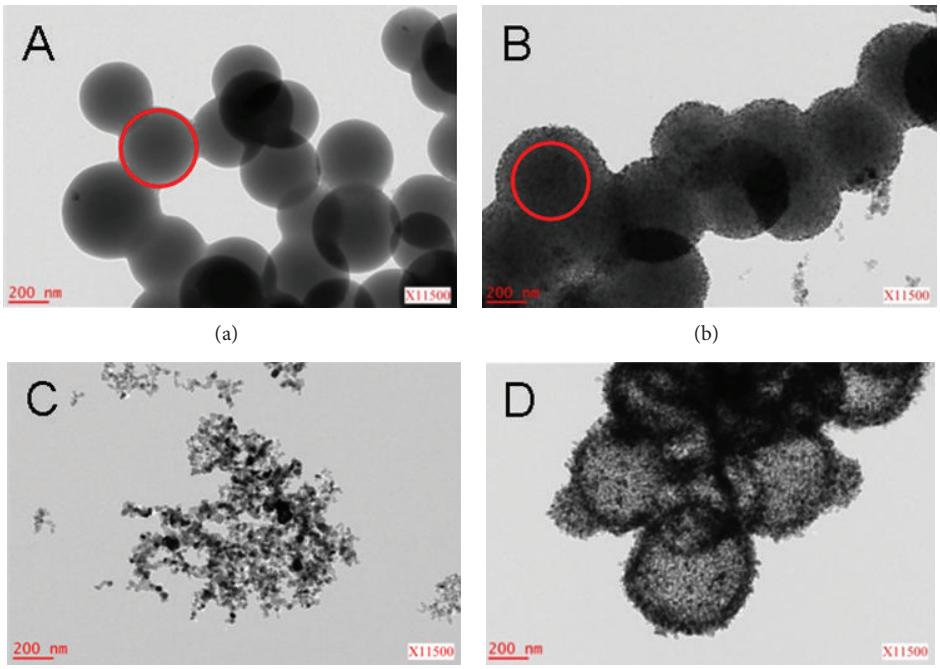

Figure 2: TEM images of the (a) carbon spheres, (b) core/shell carbon/titania composite, (c) P25, and (d) titania hollow spheres.

(Figure 2(d)), where the wall is constituted of TiO_2 particles with an estimated thickness of about 50–60 nm. The TEM images show that there was neither structural collapse nor sintering of titania particles during the calcination step.

The XRD patterns of the samples (Figure 3(a)) confirmed that anatase is the dominant crystalline phase in the titania particles, with the well-defined characteristic peaks at 25.3°, 37.8°, and 48°. In the case of the carbon/titania composite the broad band between 20° and 25°, characteristic of the reflections associated to amorphous carbon was also evident. Based on the larger intensity of the diffraction peaks, it might also be inferred that the crystallinity is higher in P25 than in samples CSTi and HSTi. The optical properties of the samples were also explored by UV-Vis diffuse reflectance spectroscopy; the spectral differences are more evident in the Tauc plots shown in Figure 3(b) [24]. The spectrum of P25 presented the characteristic absorption sharp edge of the anatase form of TiO_2 (predominant phase) in the UV region raising above 400 nm (onset wavelength at about 380 nm). For CSTi, a pronounced increase in the absorption between 400 and 800 nm (visible range) was observed due to the carbon matrix; this has been attributed as either the presence of photosensitive functional groups on the carbon matrix [17] or the light absorption capacity of the carbon matrix itself [25, 26]. The carbon doping seems to modify the optical response of titanium dioxide as a slight red shift was observed in the DRUV spectrum of CSTi compared to HSTi. What is also interesting to remark is that the optical absorption bands of the titania hollow spheres are very close to that of commercial powders (sample P25), with the onset slightly shifted towards longer wavelengths.

3.2. Photoelectrochemical Response. To investigate the effect of the morphology on the photoelectrochemical response of titania particles, photocurrent response experiments were carried out under UV pulsed irradiation cycles on the thin film electrodes casted on ITO slides. Due to the resistive character of the carbon spheres, the photogenerated current detected for the carbon/titania composite was extremely low (tens of microamperes) and could not be accurately and reproducibly detected. Consequently, only those results corresponding to HSTi and P25 were evaluated and will be discussed.

Voltammetry was employed to study the effect of the potential bias on the photocurrent response under UV illumination of the catalysts. Similar photoelectrochemical responses were obtained for both electrodes built on P25 and HSTi (see example in Figure 4(a) corresponding to sample HSTi), showing the characteristic shape of photocurrent-potential curves of an n-type semiconductor. At dark conditions, two distinctive regions are observed depending on the applied potential. Below −0.3 V versus SCE, the cathodic current corresponds to the flux of electrons located in the accumulation region that appears at the interface semiconductor/electrolyte; above this potential value, the voltammograms show a flat signal corresponding to the depletion region where the current cannot flow and the electrode behaves like a diode.

Upon UV illumination, an anodic photocurrent appeared in both thin film electrodes (onset at ca. −0.4 V versus SCE) showing saturation at about 0 V versus SCE. This photocurrent arises from the separation of the photogenerated charge carriers (e^-/h^+) at the TiO_2/electrolyte interface. In such conditions, the holes are readily reduced by

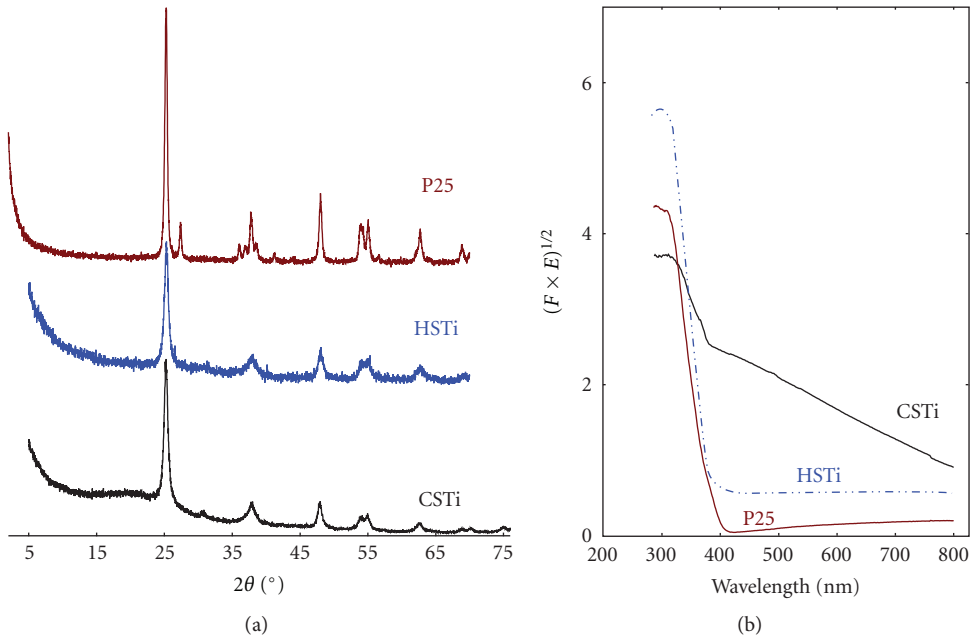

FIGURE 3: (a) XRD patterns of the core/shell carbon/titania composite, P25, and titania hollow spheres; (b) Tauc representation of the UV-Vis diffuse spectra of the studied photocatalysts.

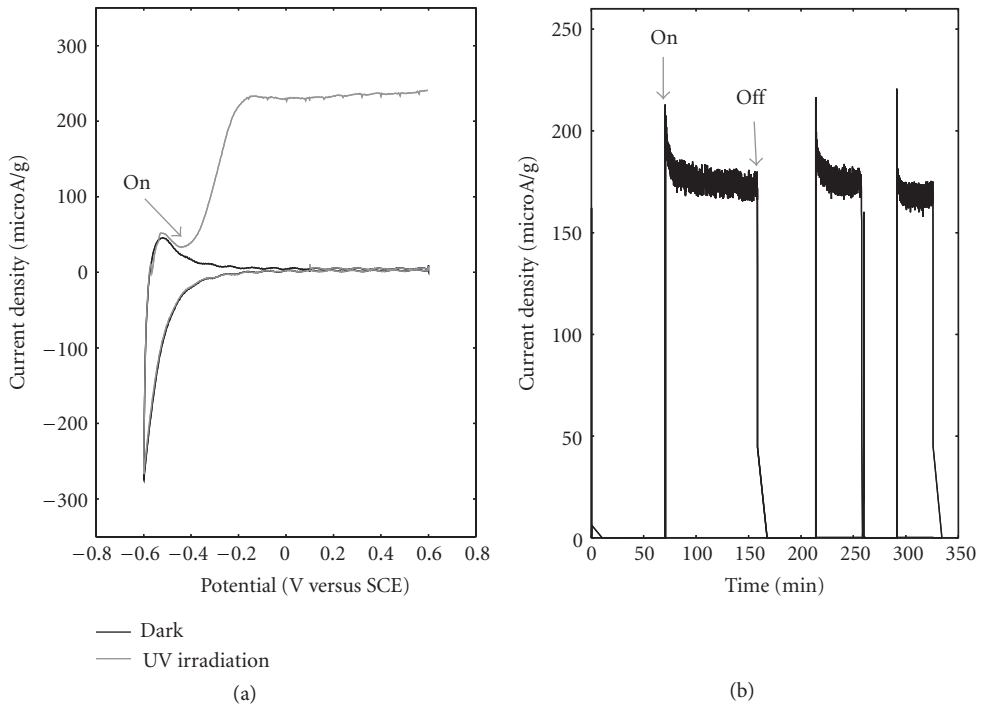

FIGURE 4: Photoelectrochemical behavior. (a) Cyclic voltammetry and (b) on-off illumination cycles at a fixed bias potential of +0.5 V versus SCE of the hollow sphere titania electrode.

an electron donor present in the electrolyte (i.e., H_2O) [27], while the photogenerated electrons are effectively transferred through TiO_2 grain boundaries to the counter electrode via the external circuit. In the low potential region, the separation between electrons and holes is in a rate-limiting process, thus the photocurrent increases with the applied potential. The photocurrent saturates at higher bias potentials (above 0 V versus SCE) due to limitation of the photohole capture process at the TiO_2 surface [28].

The transient photocurrent response upon on-off illumination cycles was also recorded for both samples. Figure 4(b) shows the characteristic curve obtained for an applied bias potential of ca. +0.5 V versus SCE. Again a similar photoelectrochemical response was obtained for both electrodes; as the photochemical behavior of titania greatly depends on the efficiency of electron-hole pair excitation, the electron-hole transfer, and the electron-hole pairs separation, these results anticipate a similar photocatalytic activity in both titania samples when exposed to light.

The photoelectrochemical response was characterized by a prompt increase in the photocurrent upon illumination, which retracted to original values almost instantaneously once the illumination was turned off. Quantitatively, small differences were detected in the photocurrent density for both thin film electrodes; according to the literature, these are likely attributed to the variation in the thickness of the film electrodes [29–31]. On the other hand, this effect could also be attributed to the lower crystallinity of the anatase phase in the hollow spheres compared to P25 (Figure 3(a)).

3.3. Photocatalytic Activity towards Phenol Degradation. Phenol adsorption studies under dark conditions were performed for all three studied catalysts using the same operating conditions described for the photocatalytic experiments. This approach allowed to discriminate the fraction of photooxidized (degraded) pollutant in the catalytic reaction from that removed by adsorption when no irradiation applies (dark conditions). Obtained data showed that the amount of phenol adsorbed for P25 is almost negligible (below ca. 3%), and it accounts for ca. 7% in the case of HSTi and CSTi. These values are consistent with the low surface area and pore volumes of the catalysts as measured by gas adsorption (Table 1). In all cases, the contribution of adsorption to the overall phenol removal efficiency is very small for the three studied catalysts. It should also be pointed out that since the immobilization of the titania layer on the carbon matrix was based on chemical grafting on the O-surface groups that decorate the carbon surface, no leaching out of the photoactive particles was detected from solution during the photodegradation experiments at any time.

Data corresponding to phenol photolysis (noncatalyzed reaction) has also been included for comparison reasons. Under herein reported irradiation conditions (i.e., lamp characteristics, phenol initial concentration, and solution pH), the photolytic breakdown of phenol was noticeable, with a large decrease in phenol concentration with time comparable to that obtained in the photocatalytic reactions (Table 2). However, analysis of the total organic carbon (TOC) content of the solution indicated that—despite the decrease in phenol concentration—almost no mineralization (i.e., phenol conversion to CO_2 + H_2O) was achieved by direct interaction with UV light. Phenol photolysis led to rising amounts of catechol (CAT), hydroquinone (HY), benzoquinone (BZ), and short alkyl-chain organic acids (SOA) as main degradation intermediates (Table 2).

On the other hand, the rate of phenol degradation upon irradiation was very similar for the three catalysts (data not shown) although some differences were observed in the overall catalytic yields (Table 2). Indeed, the TOC values corresponding to the solution after 6 h of irradiation were similar for both CSTi and HSTi samples (i.e., 44 and 43 mg C/L, resp.). Moreover, these catalysts also promoted a higher mineralization of phenol than P25 through its conversion to CO_2 + H_2O, as evidenced in Table 2. Bearing in mind the low contribution of adsorption to the overall process (as abovementioned) for all three catalysts, these findings confirm the better photocatalytic performance of samples CSTi and HSTi compared to bulk P25. This behavior must be interpreted in terms of the structure and composition of the catalysts, rather than their porosity. This points out an interesting viewpoint on the role of the crystallinity and the morphology of photocatalysts with similar chemical composition (i.e., TiO_2), as major factors governing the photocatalytic activity of titania-based materials (i.e., P25 versus HSTi).

Speciation of the degradation intermediates found in solution indicated the predominance of organic acids (Table 2) over aromatic intermediates (Figure 5) for all the samples. What is more interestingly inferred is that the relative abundance of the aromatic intermediates depends on the catalyst (Figure 5). For instance, large amounts of BZ and HY are detected when P25 is irradiated (compared to HSTi and CSTi), which is in good agreement with reported works in the literature for this material [32]. On the other hand, the intermediate evolution of the composite and the hollow spheres are quite similar. This points out the higher photocatalytic activity of the titania particles in a sphere morphology.

Since the photocatalytic performance of CSTi and HSTi are similar, in terms of mineralization and conversion, the presence of the carbon phase in the composite does not seem to play an important role affecting the photooxidation

Table 2: TOC values (mg C/L) in solution after 6 hours (initial TOC values were 76 mg C/L in all the cases) with indication of the relative abundance of phenol and its degradation intermediates, and the overall conversion in terms of phenol degradation and mineralization yields (%).

(a) Solution composition after 6 h of irradiation

	Phenol[a]	HY + BZ + CAT[a*]	SOA[a*]	Total TOC (mg C/L)
P25	0.31	0.08	0.61	51.3
CSTi	0.53	0.04	0.43	44.2
HSTi	0.47	0.03	0.50	43.4
Photolysis	0.19	0.07	0.74	73.6

[a]Relative abundance versus TOC values.
*HY: hydroquinone; BZ: benzoquinone; CAT: catechol; SOA: short alkyl chain organic acids.

(b) Overall photocatalytic conversion

	Degraded phenol (%)	Mineralization (%)
P25	79	33
CSTi	69	42
HSTi	73	43
Photolysis	82	3

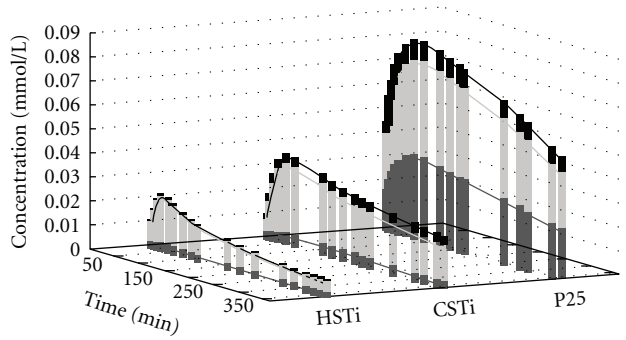

Figure 5: Evolution of phenol aromatic degradation intermediates detected in solution upon UV irradiation of the photocatalysts. From bottom to top: HY (dark grey), BZ (light grey), and CAT (black).

efficiency (compared to HSTi). These findings contrast with previous studies in the literature addressing the beneficial effect of carbon as a support on the photocatalytic performance of semiconductors ([9, 10] and the references therein), and attributing it to single and collective factors based on the combination of the photoactivity of the immobilized semiconductor and the structural, textural, and electronic features of the carbon support (including the self photoactivity of certain carbon phases [13] and the role of O-containing surface groups of the carbon acting as charge injectors [33]).

Firstly, the improved photoactivity due to the contribution of confinement effects (adsorption) applies for both HSTi and CSTi, as they show similar porous features (Figure 1). So even though both samples outperform P25 (displaying a lower porosity), the positive effect (if any) of the carbon layer on CSTi over HSTi is not clear. Secondly, the plausible role of the O-containing groups of the carbon as charge injectors would be effectively suppressed here since the titania layer in CSTi is grafted on the O-moieties of the carbon spheres (chemical grafting could reduce the electron density of the oxygen atoms). Finally, the contribution of the self photoactivity provided by the carbon phase cannot be clearly demonstrated with the conventional photocatalytic tests herein reported [13]; this issue remains under investigation in our research group.

Summarizing, it seems that none of the plausible mechanisms explaining the role of carbon on the enhanced photocatalytic activity of carbon/titania composites would apply (or dominate) for CSTi; consequently, it is uncertain whether if the carbon phase has any effect on the photocatalytic response of the composite, or if this effect remains unnoticed behind that of the titania particles morphology.

On the other hand, according to XRD patterns, samples of CSTi and HSTi present lower crystallinity than commercial titania powders (Figure 3(a)), for which a better catalytic performance would have been expected for P25. However, our results indicate that the higher photocatalytic performance of titania hollow spheres cannot be explained in terms of the crystallinity of the anatase phase. Some other factors including the size and morphology of titania particles, the degree of aggregation, and the absorption characteristics might likely be responsible for the enhanced photocatalytic activity. In this regard, the small differences in the absorption characteristics observed for the catalysts (Figure 3(b)) are not expected to account for this behavior—the increase in the ability of HSTi and CSTi to harvest a higher fraction of light seems too small—which should be then explained in terms of the morphology and composition.

It is interesting to point out that the morphology of the titania layer on samples of CSTi and HSTi (which showed similar photocatalytic activity) is expected to be similar based on the synthetic procedure. In both cases it consists of a thin titania layer arranged in a spherical configuration, which in the case of CSTi is surrounded by a carbon core (dense) whereas for HSTi the main cavity is empty (hollow).

As for the different behavior inferred from the photoelectrochemical tests (where HSTi and P25 behave similarly) and the photocatalytic experiments (where HSTi outperforms P25), one has to consider that the thin film electrodes enable a fast and efficient separation of the photo-induced species, which are rapidly captured, reducing the interface recombination and decreasing the surface charge trap-site density. In contrast, in the photocatalytic experiments, the situation is more complex due to the increased probability of losses due to recombination processes and light scattering (powders are suspended in the solution).

According to the literature, intergrain boundaries (particle connections) increase the probability of recombination as they can behave as electron trap states [34]. This is more likely to happen in bulk titania powders (P25) where resistances associated to intergrain boundaries are expected to be higher than in the mesoporous hollow inner structure of HSTi particles [34]. The adequate morphology of HSTi due to an accessible mesoporous configuration at the spherical surface would favor the motion of the charge carriers and the electron conductivity through the surface of titania particles (despite the poor electron conductivity of TiO_2 itself) [35–37]. The hollow inner structure of HSTi has also been reported to enhance the light harvesting in the porous voids, and thus increasing the quantity of photogenerated electrons and holes to participate in the photocatalytic decomposition reactions [38, 39]. All these features are key aspects leading to higher catalytic activity of hollow structures over large particles [40].

Finally, it is interesting to remark that an efficient photocatalyst should not only show high photocatalytic activity, but also lead to easy recovery from the solution. In this regard, while the solution after the treatment with P25 or HSTi has substantial turbidity, a fast and easy sedimentation was observed for the carbon/titania core shell composite. This fact is of primary importance since it makes possible the complete recovery and reutilization of the material. Similar observations on the positive effect of carbon supports on the decantability and the so-called practical efficiency of carbon/semiconductor photocatalysts have been reported elsewhere [25]. Better photocatalytic efficiencies were achieved with HSTi and CSTi, since the greatest difference in the performance of both catalysts relies on their recovery after the experiments, a higher practical efficiency is achieved in the case of the carbon : titania core shells (which are more easily

decantable). This represents a clear advantage for the large scale implementation of the process, thus the carbon/titania composite may be considered a promising candidate for useful photocatalysts.

4. Conclusions

This paper describes the photocatalytic response of mesoporous titania particles with spherical morphology arranged in two different configurations: hollow and core/shell structures, where the titania layer is surrounding a carbon core. The carbon matrix was used as a morphology director during the synthesis of the titania film in samples of CSTi and HSTi, and as a scaffold to prevent the structural collapse and sintering of titania particles during calcination. Anatase was the dominant crystalline phase for the synthesized catalysts, although the XRD patterns showed lower crystallinity compared to commercial titania powders. The mesoporous titania particles in an spherical arrangement also showed similar optical and photoelectrochemical response than P25; however, the absorption properties were largely modified after the incorporation of the carbon matrix (CSTi), with a pronounced increase in the absorption region corresponding to the visible range.

Herein synthesized catalysts showed higher photocatalytic efficiency towards phenol photooxidation than commercial titania powders. Considering their physicochemical, optical, and structural properties, the increase in the mineralization efficiency might be connected to the adequate morphology of the titania particles (both in the hollow and core/shell arrangements) along with the accessible mesoporosity. The morphology of the semiconductor layer favors the fast motion of the charge carriers and the electron conductivity through the surface of the titania particles; recombination phenomena are also minimized due to the lower density of intergrain boundaries in these materials, which results in the enhanced photocatalytic response.

The incorporation of the carbon phase in the core/shell composite increases the practical efficiency of the catalyst, due to the better decantability and improved separation from the reaction medium and given that the spherical mesoporous morphology of the titania layer is preserved. We believe this is an important parameter to be taken into account for the implementation of the photocatalysis to environmental remediation.

Acknowledgments

The authors thank the financial support of the Spanish MICINN and FICYT (Grants CTM2008/01956, CTM2011/02338, and PC10-002). L. F. Velasco and M. Haro thank CSIC for financial support (JAE-Pre and JAE-Doc contracts).

References

[1] D. F. Ollis and H. Al-Elkabi, *Photocatalytic Purification and Treatment of Water and Air*, Elsevier, Amsterdam, The Netherlands, 1993.

[2] M. A. Henderson, "A surface science perspective on TiO_2 photocatalysis," *Surface Science Reports*, vol. 66, no. 6-7, pp. 185–297, 2011.

[3] N. Serpone and E. Pelizzetti, *Photocatalysis: Fundamental and Applications*, Wiley-Interscience, New-York, NY, USA, 1983.

[4] A. L. Linsebigler, G. Lu, and J. T. Yates, "Photocatalysis on TiO_2 surfaces: principles, mechanisms, and selected results," *Chemical Reviews*, vol. 95, no. 3, pp. 735–758, 1995.

[5] M. I. Litter and J. A. Navío, "Photocatalytic properties of iron-doped titania semiconductors," *Journal of Photochemistry and Photobiology A*, vol. 98, no. 3, pp. 171–181, 1996.

[6] S. Sakthivel and H. Kisch, "Daylight photocatalysis by carbon-modified titanium dioxide," *Angewandte Chemie—International Edition*, vol. 42, no. 40, pp. 4908–4911, 2003.

[7] Y. Cho, W. Choi, C. H. Lee, T. Hyeon, and H. I. Lee, "Visible light-induced degradation of carbon tetrachloride on dye-sensitized TiO_2," *Environmental Science and Technology*, vol. 35, no. 5, pp. 966–970, 2001.

[8] A. Fernández, G. Lassaletta, V. M. Jiménez et al., "Preparation and characterization of TiO_2 photocatalysts supported on various rigid supports (glass, quartz and stainless steel). Comparative studies of photocatalytic activity in water purification," *Applied Catalysis B: Environmental*, vol. 7, no. 1-2, pp. 49–63, 1995.

[9] R. Leary and A. Westwood, "Carbonaceous nanomaterials for the enhancement of TiO_2 photocatalysis," *Carbon*, vol. 49, no. 3, pp. 741–772, 2011.

[10] J. L. Faria and W. H. Wang, "Carbon materials in photocatalysis," in *Carbon Materials for Catalysis*, P. Serp and J. L. Figueiredo, Eds., chapter 13, John Wiley & Sons, New York, NY, USA, 2009.

[11] J. Matos, J. Laine, and J. M. Herrmann, "Synergy effect in the photocatalytic degradation of phenol on a suspended mixture of titania and activated carbon," *Applied Catalysis B*, vol. 18, no. 3-4, pp. 281–291, 1998.

[12] L. F. Velasco, J. B. Parra, and C. O. Ania, "Role of activated carbon features on the photocatalytic degradation of phenol," *Applied Surface Science*, vol. 256, no. 17, pp. 5254–5258, 2010.

[13] L. F. Velasco, I. M. Fonseca, J. B. Parra, J. C. Lima, and C. O. Ania, "Photochemical behavior of activated carbons under UV irradiation," *Carbon*, vol. 50, no. 1, pp. 249–258, 2012.

[14] M. Inagaki, N. Kondo, R. Nonaka et al., "Structure and photoactivity of titania derived from nanotubes and nanofibers," *Journal of Hazardous Materials*, vol. 161, no. 2-3, pp. 1514–1521, 2009.

[15] W. Shen, Y. Zhu, X. Dong, J. Gu, and J. Shi, "A new strategy to synthesize TiO_2-hollow spheres using carbon spheres as template," *Chemistry Letters*, vol. 34, no. 6, pp. 840–841, 2005.

[16] R. B. Zheng, X. W. Meng, and F. Q. Tang, "A general protocol to coat titania shell on carbon-based composite cores using carbon as coupling agent," *Journal of Solid State Chemistry*, vol. 182, no. 5, pp. 1235–1240, 2009.

[17] J. Matos, A. García, L. Zhao, and M. M. Titirici, "Solvothermal carbon-doped TiO_2 photocatalyst for the enhanced methylene blue degradation under visible light," *Applied Catalysis A*, vol. 390, no. 1-2, pp. 175–182, 2010.

[18] J. Liu, G. Zhang, W. Ao, K. Yang, S. Peng, and C. Müller-Goymann, "Hollow mesoporous titania microsphere with low shell thickness/diameter ratio and high photocatalysis," *Applied Surface Science*, vol. 258, no. 20, pp. 8083–8089, 2012.

[19] Y. H. Ao, J. J. Xu, D. G. Fu, and C. W. Yuan, "Visible-light responsive C,N-codoped Titania hollow spheres for X-3B dye photodegradation," *Microporous and Mesoporous Materials*, vol. 118, no. 1-3, pp. 382–386, 2009.

[20] X. Wang, H. He, Y. Chen, J. Zhao, and X. Zhang, "Anatase TiO_2 hollow microspheres with exposed {001} facets: facile synthesis and enhanced photocatalysis," *Applied Surface Science*, vol. 258, no. 15, pp. 5863–5868, 2012.

[21] J. S. Noh and J. A. Schwarz, "Estimation of the point of zero charge of simple oxides by mass titration," *Journal of Colloid And Interface Science*, vol. 130, no. 1, pp. 157–164, 1989.

[22] X. Sun and Y. Li, "Colloidal carbon spheres and their core/shell structures with noble-metal nanoparticles," *Angewandte Chemie—International Edition*, vol. 43, no. 5, pp. 597–601, 2004.

[23] M. Sevilla and A. B. Fuertes, "Chemical and structural properties of carbonaceous products obtained by hydrothermal carbonization of saccharides," *Chemistry—A European Journal*, vol. 15, no. 16, pp. 4195–4203, 2009.

[24] R. López and R. Gómez, "Band gap energy estimation from diffuse reflectance measurements on sol-gel and commercial TiO_2: a comparative study," *Journal of Sol-Gel Science and Technology*, vol. 61, no. 1, pp. 1–7, 2012.

[25] J. Araña, J. M. Doña-Rodríguez, E. Tello Rendón et al., "TiO_2 activation by using activated carbon as a support: part II. Photoreactivity and FTIR study," *Applied Catalysis B*, vol. 44, no. 2, pp. 153–160, 2003.

[26] L. F. Velasco, J. B. Parra, and C. O. Ania, "Phenol adsorption and photo-oxidation on porous carbon/titania composites," *Adsorption Science and Technology*, vol. 28, no. 8-9, pp. 727–738, 2010.

[27] M. Yang, L. H. Li, S. Q. Zhang, G. Y. Li, and H. J. Zhao, "Preparation, characterisation and sensing application of inkjet-printed nanostructured TiO_2 photoanode," *Sensors and Actuators B*, vol. 147, no. 2, pp. 622–628, 2010.

[28] D. L. Jiang, H. J. Zhao, S. Q. Zhang, and R. John, "Characterization of photoelectrocatalytic processes at nanoporous TiO_2 film electrodes: photocatalytic oxidation of glucose," *Journal of Physical Chemistry B*, vol. 107, no. 46, pp. 12774–12780, 2003.

[29] T. Lana-Villarreal, Y. B. Mao, S. S. Wong, and R. Gómez, "Photoelectrochemical behaviour of anatase nanoporous films: effect of the nanoparticle organization," *Nanoscale*, vol. 2, no. 9, pp. 1690–1698, 2010.

[30] J. G. Yu, X. J. Zhao, and Q. N. Zhao, "Effect of film thickness on the grain size and photocatalytic activity of the sol-gel derived nanometer TiO_2 thin films," *Journal of Materials Science Letters*, vol. 19, no. 12, pp. 1015–1017, 2000.

[31] S. C. Jung, S. J. Kim, N. Imaishi, and Y. I. Cho, "Effect of TiO_2 thin film thickness and specific surface area by low-pressure metal-organic chemical vapor deposition on photocatalytic activities," *Applied Catalysis B*, vol. 55, no. 4, pp. 253–257, 2005.

[32] E. B. Azevedo, A. R. Tôrres, F. R. A. Neto, and M. Dezotti, "TiO_2-photocatalyzed degradation of phenol in saline media in an annular reactor: hydrodynamics, lumped kinetics, intermediates, and acute toxicity," *Brazilian Journal of Chemical Engineering*, vol. 26, no. 1, pp. 75–87, 2009.

[33] R. Ocampo-Pérez, M. Sánchez-Polo, J. Rivera-Utrilla, and R. Leyva-Ramos, "Enhancement of the catalytic activity of TiO_2 by using activated carbon in the photocatalytic degradation of cytarabine," *Applied Catalysis B*, vol. 104, no. 1-2, pp. 177–184, 2011.

[34] T. Berger, T. Lana-Villarreal, D. Monllor-Satoca, and R. Gómez, "An electrochemical study on the nature of trap states in nanocrystalline rutile thin films," *Journal of Physical Chemistry C*, vol. 111, no. 27, pp. 9936–9942, 2007.

[35] M. Kaneko, S. Suzuki, H. Ueno, J. Nemoto, and Y. Fujii, "Photoelectrochemical decomposition of bio-related compounds at a nanoporous semiconductor film photoanode and their photocurrent-photovoltage characteristics," *Electrochimica Acta*, vol. 55, no. 9, pp. 3068–3074, 2010.

[36] A. Syoufian, O. H. Satriya, and K. Nakashima, "Photocatalytic activity of titania hollow spheres: photodecomposition of methylene blue as a target molecule," *Catalysis Communications*, vol. 8, no. 5, pp. 755–759, 2007.

[37] J. G. Yu and J. Zhang, "A simple template-free approach to TiO_2 hollow spheres with enhanced photocatalytic activity," *Dalton Transactions*, vol. 39, no. 25, pp. 5860–5867, 2010.

[38] J. G. Yu and X. X. Yu, "Hydrothermal synthesis and photocatalytic activity of zinc oxide hollow spheres," *Environmental Science and Technology*, vol. 42, no. 13, pp. 4902–4907, 2008.

[39] J. G. Yu and G. H. Wang, "Hydrothermal synthesis and photocatalytic activity of mesoporous titania hollow microspheres," *Journal of Physics and Chemistry of Solids*, vol. 69, no. 5-6, pp. 1147–1151, 2008.

[40] H. Bala, Y. H. Yu, and Y. H. Zhang, "Synthesis and photocatalytic oxidation properties of titania hollow spheres," *Materials Letters*, vol. 62, no. 14, pp. 2070–2073, 2008.